Pergamon

Int. J. Heat Mass Transfer. Vol. 40, No. 11, pp. 2721–2738, 1997

Printed in Great Britain
0017-9310/97 $17.00+0.00

PII: S0017-9310(96)00213-X

Investigation of transport equations for turbulent heat fluxes in compressible flows

C. LE RIBAULT and R. FRIEDRICH†

Lehrstuhl für Fluidmechanik, Technische Universität München, Arcisstrasse 21, 80290 München, Germany

(*Received* 13 *June* 1995 *and in final form* 23 *February* 1996)

Abstract—Turbulent heat fluxes are usually modeled by algebraic relations containing the turbulent Prandtl number. The underlying hypothesis of an analogy between turbulent momentum and heat transport is, however, not valid in complex flow situations. Transport equations are then needed to predict the heat fluxes. Two such equations are implemented in a code for statistically two-dimensional flows with a Reynolds stress model. The behaviour of this SOC model is tested in cases of compressible boundary layers along adiabatic walls at different Mach numbers and for hypersonic boundary layers along cooled walls. Finally, shock/turbulent boundary layer interactions are computed and discussed. © 1997 Elsevier Science Ltd. All rights reserved.

INTRODUCTION

The accurate prediction of compressible turbulent flows is still a challenging task for the aerodynamicist and achieves increasing importance with plans by aerospace companies to develop a new generation of passenger aircraft, the High Speed Civil Transport (HSCT). The key to successfully developing such an aircraft is new materials for both engines and airframe, but also the knowledge about heat loads which are highest when the flow is turbulent.

Turbulent heat fluxes generated in high speed flows are mostly modeled using the Boussinesq hypothesis, i.e. postulating constant turbulent Prandtl numbers or specific profiles. In complex flow situations with varying pressure gradients or in shock/turbulent boundary layer interactions the turbulent Prandtl number cannot be prescribed *a priori* because it changes in space in a complicated way. In order to improve the prediction of heat transfer, transport equations for the turbulent heat fluxes are needed.

In the past efforts have been made to improve the closure of transport equations for the Reynolds stresses in the case of compressible flows, but no such efforts are known of with respect to turbulent heat fluxes. A reason may be the lack of experimental data and the enormous difficulties in accurately measuring these quantities when the flow is compressible. Existing studies of turbulent flows involving heat transport are related to incompressible flows. Two types of more sophisticated models have been developed: models using transport equations for the turbulent heat fluxes (Lai and So [1], Mompean [2]) and models involving transport equations for the variance of the temperature fluctuation and its dissipation rate (Sommer [3], Lai and So [1], Mompean [2]). In the second case, the turbulent heat fluxes are again computed via a Boussinesq hypothesis, but the thermal eddy diffusivity is related to these two quantities. The low Reynolds number model developed by Lai and So is of the first type and takes the near wall asymptotic behaviour of each term in the heat flux transport equations into account. It has been adopted in the present investigation, assuming that intrinsic effects of compressibility are of minor importance in the flows studied.

A low Reynolds number SOC model based on transport equations for the Reynolds stresses and the turbulent energy dissipation rate had already been applied to complex compressible flows by Haidinger [4], Haidinger and Friedrich [5, 6]. In the present work, two transport equations for the turbulent heat fluxes in statistically two-dimensional situations are added and modeled. The performance of these equations is studied in the case of compressible flows through comparisons with algebraic models and experimental results.

In the paper, the exact equations for the turbulent heat fluxes and their modeled versions are first presented. Then, the method of numerical integration is briefly described. Computations of turbulent boundary layers along adiabatic walls at different Mach numbers and along cooled walls have been performed and discussed. More complex flow cases such as shock/boundary layer interactions are finally analyzed.

2. REYNOLDS STRESS MODEL

In refs. [4, 5] a Reynolds stress model has been applied to compressible flows. A gradient transport hypothesis served to model the turbulent heat fluxes.

† Author to whom correspondence should be addressed.

NOMENCLATURE

a speed of sound
b_{ij} Reynolds stress anisotropy tensor
$C_1, C_2, C_3, C_4, C_5, C_1^*, C_5^*, C_S, C_\mu$ model constants [equations (8) and (27)]
$C_\theta, C_{1\theta}, C_{2\theta}, C_{1\theta,\omega}, C_5^\theta, C_{\varepsilon 1}, C_{\varepsilon 2}$ model constants [equations (8) and (27)]
D_{ij}^μ, D_{ij}^t molecular and turbulent diffusion terms
$F(Ma_T)$ empirical model function
fw wall damping function
$\tilde{h}, h'$ Favre averaged and fluctuating enthalpy
$\overline{h'\partial p/\partial x_i}$ pressure-scrambling term
k turbulent kinetic energy
Ma_T turbulent Mach number
n_i unit normal to (and with the origin at) the wall
Re_t turbulent Reynolds number $k^2/\nu\varepsilon$
p pressure
P_{ij} production tensor
$\overline{p''\partial u_k'/\partial x_k}$ pressure-dilatation correlation
Pr Prandtl number
q_j heat flux vector
t time
u' fluctuating streamwise velocity
$\tilde{u}_i, u_i'$ ith component of the Favre averaged and fluctuating velocity
$\widetilde{u_i'u_j'}$ Reynolds stress tensor
$\widetilde{u_i'h'}$ turbulent heat flux vector
x_i Cartesian coordinate (x_1 streamwise, x_2, y normal to the wall)
w' fluctuating velocity normal to the wall.

Greek symbols
$\alpha, \alpha_1, \alpha_2$ model constants [equations (8), (15)]
δ_{ij} Kronecker delta
ε_c dilatational or compressible dissipation rate
ε_s solenoidal dissipation rate
ε_{ij} turbulent dissipation rate tensor
μ molecular shear viscosity
μ_T eddy viscosity
$\bar{\rho}, \rho$ mean and instantaneous mass density
$\sigma_\varepsilon, \sigma_\rho$ model constants [equations (8), (15)]
τ_{ij} shear stress tensor
$\Phi_i, \Phi_{i,1}, \Phi_{i,2}, \Phi_{i,3}, \Phi_{i,w}$ parts of the model for the pressure scrambling term
Φ_{ij} pressure strain correlation tensor
ω specific dissipation rate.

Superscripts
$\overline{(..)}$ Reynolds average
$\tilde{(..)}$ Favre average
$''$ Reynolds fluctuation
$'$ Favre fluctuation.

Besides this a two equations (k–ω) model has been tested in complex compressible flow cases like shock/boundary layer interactions. It is based on Wilcox's formulation [7] which accounts for the pressure-dilatation correlation and the compressible dissipation rate in the k-equation, but it uses Zeman's formula [8, 9] for the latter instead of Wilcox's own proposal. The main advantage of choosing the ω-equation to compute the incompressible part of the turbulent dissipation rate is the possibility to compute the flow field down to the wall and have an asymptotically correct near-wall boundary condition for ω. In the case of the Reynolds stress transport equations the pressure-strain correlation is modeled according to Speziale *et al.* [10] while an isotropized version of the Hanjalic and Launder [11] model for the turbulent diffusion and the assumption of a locally isotropic turbulent dissipation rate have been adopted. The complete set of modeled Reynolds stress and turbulent dissipation equations reads:

$$\frac{\partial \bar{\rho}\widetilde{u_i'u_j'}}{\partial t} + \frac{\partial \bar{\rho}\widetilde{u_i'u_j'}\,\tilde{u}_k}{\partial x_k} + P_{ij} + D_{ij}^t$$

$$- D_{ij}^\mu - \phi_{ij} - \frac{2}{3}\overline{p''\frac{\partial u_k'}{\partial x_k}}\delta_{ij} + \bar{\rho}\varepsilon_{ij} = 0 \quad (1)$$

with the production term:

$$P_{ij} = \bar{\rho}\widetilde{u_i'u_k'}\frac{\partial \tilde{u}_j}{\partial x_k} + \bar{\rho}\widetilde{u_j'u_k'}\frac{\partial \tilde{u}_i}{\partial x_k}. \quad (2)$$

The molecular and turbulent diffusion terms are written as:

$$-D_{ij}^\mu + D_{ij}^t = -\frac{\partial}{\partial x_k}\left[\left(\bar{\mu} + \frac{2}{3}\frac{Cs}{C_\mu}\mu_T\right)\right.$$

$$\left.\times\left(\frac{\partial \widetilde{u_i'u_j'}}{\partial x_k} + \frac{\partial \widetilde{u_i'u_k'}}{\partial x_j} + \frac{\partial \widetilde{u_j'u_k'}}{\partial x_i}\right)\right]. \quad (3)$$

The pressure strain correlation according to ref. [10] is:

$$\Phi_{ij} = C_1 C_\mu \bar{\rho}\omega k b_{ij} - C_2 C_\mu \bar{\rho}\omega k(b_{ik}b_{jk} - \tfrac{1}{3}b_{mn}b_{mn}\delta_{ij})$$

$$-C_1^*\bar{\rho}\widetilde{u_m''u_n''}\frac{\partial\tilde{u}_m}{\partial x_n}b_{ij}$$
$$-C_3\bar{\rho}k\frac{1}{2}\left[b_{ik}\left(\frac{\partial\tilde{u}_j}{\partial x_k}+\frac{\partial\tilde{u}_k}{\partial x_j}\right)+b_{jk}\left(\frac{\partial\tilde{u}_i}{\partial x_k}+\frac{\partial\tilde{u}_k}{\partial x_i}\right)\right.$$
$$\left.-\frac{2}{3}b_{mn}\left(\frac{\partial\tilde{u}_m}{\partial x_n}+\frac{\partial\tilde{u}_n}{\partial x_m}\right)\delta_{ij}\right]$$
$$-C_4\bar{\rho}k\frac{1}{2}\left[b_{ik}\left(\frac{\partial\tilde{u}_j}{\partial x_k}-\frac{\partial\tilde{u}_k}{\partial x_j}\right)+b_{jk}\left(\frac{\partial\tilde{u}_i}{\partial x_k}-\frac{\partial\tilde{u}_k}{\partial x_i}\right)\right]$$
$$-(C_5-C_5^*\sqrt{b_{mn}b_{mn}})\bar{\rho}k\frac{1}{2}\left(\frac{\partial\tilde{u}_i}{\partial x_j}+\frac{\partial\tilde{u}_j}{\partial x_i}-\frac{2}{3}\frac{\partial\tilde{u}_k}{\partial x_k}\delta_{ij}\right) \quad (4)$$

and the pressure-dilatation following ref. [12] reads:

$$\overline{p''\frac{\partial u_k''}{\partial x_k}}=\alpha_1 Ma_T^2\bar{\rho}\widetilde{u_m''u_n''}\frac{\partial\tilde{u}_m}{\partial x_n}+\alpha_2 Ma_T^2 C_\mu\bar{\rho}\omega k. \quad (5)$$

The turbulent dissipation rate is split into its compressible and incompressible parts. The compressible dissipation model proposed by Zeman [8] is:

$$\bar{\rho}\varepsilon_{ij}=\frac{2}{3}\bar{\rho}(\varepsilon_s+\varepsilon_c)\delta_{ij}=\frac{2}{3}[1+\alpha F(Ma_T)]C_\mu\bar{\rho}\omega k\delta_{ij}. \quad (6)$$

For the incompressible part a transport equation for ω is solved:

$$\frac{\partial\bar{\rho}\omega}{\partial t}+\frac{\partial\bar{\rho}\omega\tilde{u}_j}{\partial x_j}+(C_{\varepsilon1}-1+\alpha_1 Ma_T^2)\frac{\omega}{k}\bar{\rho}\widetilde{u_i''u_j''}\frac{\partial\tilde{u}_i}{\partial x_j}$$
$$+[C_{\varepsilon2}-1-\alpha F(Ma_T)+\alpha_2 Ma_T^2]C_\mu\bar{\rho}\omega^2$$
$$+(C_{\varepsilon2}-1)C_\mu\sqrt{\frac{1}{2}\left(\frac{\partial\tilde{u}_i}{\partial x_j}-\frac{\partial\tilde{u}_j}{\partial x_i}\right)^2}\bar{\rho}\omega$$
$$-\frac{\partial}{\partial x_j}\left[\left(\bar{\mu}+\frac{\mu_t}{\sigma_\varepsilon}\right)\frac{\partial\omega}{\partial x_j}\right]=0. \quad (7)$$

Constants used in the model are:

$$C_\mu=0.09 \quad C_1=3.4 \quad C_1^*=1.8 \quad C_2=4.2$$
$$C_3=1.25 \quad C_4=0.4 \quad C_5=0.8 \quad C_5^*=1.3$$
$$Cs=0.07 \quad \alpha_1=0.4 \quad \alpha_2=0.2 \quad \alpha=0.75$$
$$C_{\varepsilon1}=1.56 \quad C_{\varepsilon2}=1.83 \quad \sigma_\varepsilon=2 \quad (8)$$

$$F(Ma_T)=1-\exp[-(Ma_T-0.25)^2/0.66^2] \quad \text{for } Ma_T>0.25 \quad (9)$$

$$\mu_T=\frac{\bar{\rho}k}{\omega} \quad b_{ij}=\bar{\rho}\widetilde{u_i''u_j''}/2\bar{\rho}k-\frac{1}{3}\delta_{ij}$$
$$Ma_T=\frac{\sqrt{2k}}{\bar{a}}. \quad (10)$$

The turbulent Mach number, Ma_T, is one (but not the only) measure of intrinsic effects of compressibility. The compressible part of turbulent kinetic energy dissipation rate is negligible for $Ma_T \leqslant 0.25$. In the above equations Favre's averaging has been used. Contributions from the mean velocity fluctuation, $\overline{u_i''}$, have, however, been ignored.

3. MODELING OF HEAT FLUX EQUATION

The exact transport equation for the turbulent heat flux in the case of compressible flow is:

$$\frac{\partial}{\partial t}(\bar{\rho}\widetilde{u_i''h''})+\underbrace{\frac{\partial}{\partial x_j}(\bar{\rho}\tilde{u}_j\widetilde{u_i''h''})}_{1}$$
$$=\underbrace{-\bar{\rho}\widetilde{u_j''h''}\frac{\partial\tilde{u}_i}{\partial x_j}}_{2}\underbrace{-\bar{\rho}\widetilde{u_i''u_j''}\frac{\partial\tilde{h}}{\partial x_j}}_{3}\underbrace{-\frac{\partial}{\partial x_j}(\bar{\rho}\widetilde{u_i''u_j''h''})}_{4}$$
$$\underbrace{+\overline{u_i''\frac{\partial p}{\partial t}}+\overline{u_j''u_i''\frac{\partial p}{\partial x_j}}}_{5}\underbrace{+\overline{\tau_{jk}u_i''\frac{\partial u_k}{\partial x_j}}}_{6}$$
$$\underbrace{-\overline{h''\frac{\partial p}{\partial x_i}}}_{7}\underbrace{+\overline{h''\frac{\partial\tau_{ij}}{\partial x_j}}}_{8}\underbrace{-\overline{u_i''\frac{\partial q_j}{\partial x_j}}}_{9} \quad (11)$$

where $\tau_{ij}=\mu\ (\partial u_i/\partial x_j+\partial u_j/\partial x_i)-\frac{2}{3}\mu(\partial u_k/\partial x_k)\delta_{ij}$ and $q_j=-\lambda\partial T/\partial x_j)$ represent the stress tensor for Newtonian fluids and Fourier's heat flux vector. An order of magnitude analysis of its incompressible counterpart has been done by Mompean [2] in order to select those terms which are the most important ones in high Reynolds number flow. An asymptotic analysis has also been performed by Lai and So [1] to study the asymptotic behaviour of the different terms close to the wall. The various terms in equation (11) are now discussed and modeled.

The first term represents the rate of change of the turbulent heat flux due to divergence during the mean convective transport. Terms 2 and 3 describe the production of turbulent heat flux due to mean shear and mean enthalpy gradients. All these terms can be computed directly and need no modeling.

Term 4 is a turbulent diffusion term. The analysis of Lai and So [1] shows that this term is weak near the wall and becomes more important when the Reynolds number increases. Different models have been suggested for this term. Lai and So used the model proposed by Launder [13].

$$\frac{\partial}{\partial x_j}\bar{\rho}\widetilde{u_i''u_j''h''}=-\frac{\partial}{\partial x_j}\left[C_s^\theta\frac{1}{C_\mu\omega}\bar{\rho}\left(\widetilde{u_i''u_k''}\frac{\partial\widetilde{u_j''h''}}{\partial x_k}+\widetilde{u_j''u_k''}\frac{\partial\widetilde{u_i''h''}}{\partial x_k}\right)\right]. \quad (12)$$

The constant C_s^θ is equal to 0.11. Assuming an analogy to the turbulent diffusion term in the Reynolds stress equation this term can also be modeled as:

$$\frac{\partial}{\partial x_j}\bar{\rho}\widetilde{u_i'u_j'h'} = -\frac{\partial}{\partial x_j}\left[\frac{2}{3}\frac{C_s^\theta}{C_\mu}\mu_t\left(\frac{\partial\widetilde{u_i'h'}}{\partial x_j}+\frac{\partial\widetilde{u_j'h'}}{\partial x_i}\right)\right]. \tag{13}$$

Term 5 contains compressible terms, i.e. contributions which account for compressibility of the mean and fluctuating fields. In order to model these terms correctly, data from direct numerical simulations would be very useful. Recently, Sarkar *et al.* [12] have used such data to derive models for the pressure-dilatation correlation and compressible dissipation rate. We try to express the unknown correlations in terms of models used for the Reynolds stress equation. The term $\overline{u_i'(\partial p/\partial t)}$ can be decomposed into $\overline{u_i'(\partial\bar{p}/\partial t)}$ and $\overline{u_i'(\partial p''/\partial t)}$. While the first term vanishes in statistically steady flows, the second can only be important, when the fluctuating flow exhibits considerable effects of compressibility. Both terms are neglected in the present study. Decomposing the pressure and the velocity vector into mean and fluctuating parts, the remaining term of (5) can be rewritten as:

$$\overline{u_ju_i'\frac{\partial p}{\partial x_j}} = \tilde{u}_j\overline{u_i'}\frac{\partial\bar{p}}{\partial x_j}+\tilde{u}_j\overline{u_i'\frac{\partial p''}{\partial x_j}} + \overline{u_j'u_i'}\frac{\partial\bar{p}}{\partial x_j}+\overline{u_j'u_i'\frac{\partial p''}{\partial x_j}}. \tag{14}$$

A gradient transport hypothesis can be used (see ref [14]) to model $\overline{u_i'}$ as:

$$\overline{u_i'} = \frac{\mu_t}{\sigma_\rho\bar{\rho}^2}\frac{\partial\bar{\rho}}{\partial x_i} \tag{15}$$

with $\sigma_\rho = 5$.

$\overline{u_i'u_j'(\partial p''/\partial x_j)}$ should be small compared to $\tilde{u}_j\overline{u_i'(\partial p''/\partial x_j)}$; it is therefore neglected. The correlation $\overline{u_i'(\partial p''/\partial x_j)}$ is approximated by:

$$\overline{u_i'\frac{\partial p''}{\partial x_j}} = -C_\theta\overline{p''\left(\frac{\partial u_i'}{\partial x_j}+\frac{\partial u_j'}{\partial x_i}\right)} \tag{16}$$

where C_θ is assumed to be of order 1. For the r.h.s. of (16) a modelisation is available from the Reynolds stress model. Term 6 is decomposed as:

$$\overline{\tau_{jk}u_i'\frac{\partial u_k}{\partial x_j}} = \overline{\tau_{jk}u_i'}\frac{\partial\tilde{u}_k}{\partial x_j}+\overline{\tau_{jk}u_i'\frac{\partial u_k'}{\partial x_j}} \tag{17}$$

and the second term on the r.h.s. is neglected being an order of magnitude smaller than the first one. A further decomposition of the stress tensor leads to:

$$\overline{\tau_{jk}u_i'}\frac{\partial\tilde{u}_k}{\partial x_j} = \bar{\tau}_{jk}\overline{u_i'}\frac{\partial\tilde{u}_k}{\partial x_j}+\overline{\tau_{jk}'u_i'}\frac{\partial\tilde{u}_k}{\partial x_j}. \tag{18}$$

The molecular diffusion term $\overline{\tau_{ik}'u_j'}$ also appears in the Reynolds stress transport equations. We adopt the corresponding model, writing:

$$\overline{\tau_{jk}'u_i'} = \frac{1}{2}\bar{\mu}\left(\frac{\partial\widetilde{u_i'u_j'}}{\partial x_k}+\frac{\partial\widetilde{u_i'u_k'}}{\partial x_j}+\frac{\partial\widetilde{u_j'u_k'}}{\partial x_i}\right). \tag{19}$$

Term 7 represents the pressure-scrambling term. A modelisation of this term has been described by Lai and So [1] for incompressible turbulence. The authors first split the correlation into a high Reynolds number part and a near wall part, according to:

$$\overline{h'\frac{\partial p}{\partial x_i}} = \Phi_i + fw\Phi_{i,w} \tag{20}$$

Φ_i is then decomposed into

$$\Phi_i = \Phi_{i,1}+\Phi_{i,2}+\Phi_{i,3} \tag{21}$$

where $\Phi_{i,1}$ represents the contribution due to turbulence fluctuations

$$\Phi_{i,1} = -C_{1\theta}C_\mu\omega\bar{\rho}\widetilde{u_i'h'} \tag{22}$$

$\Phi_{i,2}$ counteracts the production term

$$\Phi_{i,2} = -C_{2\theta}\bar{\rho}\widetilde{u_k'h'}\frac{\partial\tilde{u}_i}{\partial x_k} \tag{23}$$

and $\Phi_{i,3}$ is a wall reflection term

$$\Phi_{i,3} = -C_{1\theta,\omega}\bar{\rho}\widetilde{u_k'h'}n_kn_i\frac{k^{1/2}}{z}. \tag{24}$$

n_i represents the unity vector normal to the wall. Lai and So have made computations with and without this term and finally suggest to neglect this term. The influence of $\Phi_{i,3}$ will also be tested here. For the second term on the r.h.s. of (20), Lai and So's model is adopted here:

$$\Phi_{i,w} = C_{1\theta}C_\mu\omega\bar{\rho}\widetilde{u_i'h'}-C_\mu\omega\bar{\rho}\widetilde{u_k'h'}n_kn_i \tag{25}$$

The damping factor fw is:

$$fw = \exp\left(-\left(\frac{Re_t}{80}\right)^2\right). \tag{26}$$

The complete model takes care of the asymptotic flow behaviour near the wall. The different model constants are:

$$C_{1\theta} = 3.0 \quad C_{2\theta} = 0.4 \quad C_{1\theta,\omega} = 0.75 \tag{27}$$

The last two terms of equation (11) are grouped together and then decomposed in the following way:

$$\begin{aligned}-\overline{u_i'\frac{\partial q_j}{\partial x_j}}+\overline{h'\frac{\partial\tau_{ij}}{\partial x_j}} &= \overline{u_i'}\frac{\partial}{\partial x_j}\left(\frac{\bar{\mu}}{Pr}\frac{\partial\tilde{h}}{\partial x_j}\right)+\frac{\partial}{\partial x_j}\left(\frac{\bar{\mu}}{Pr}\overline{u_i'\frac{\partial h'}{\partial x_j}}\right)\\ &-\frac{\bar{\mu}}{Pr}\overline{\frac{\partial u_i'}{\partial x_j}\frac{\partial h'}{\partial x_j}}+\overline{h'}\frac{\partial\bar{\tau}_{ij}}{\partial x_j}+\frac{\partial}{\partial x_j}(\overline{h'\tau_{ij}'})-\overline{\tau_{ij}'\frac{\partial h'}{\partial x_j}}.\end{aligned} \tag{28}$$

The terms $\overline{u_i'}$ and $\overline{h'}$ reflect compressibility effects in the fluctuating fields. While $\overline{u_i'}$ is modelled according to equation (15), h' is neglected. The second and fifth terms on the r.h.s. of (28) are diffusion terms, whereas the third and sixth terms are dissipation terms. They

are modelled in a way similar to the ones proposed by Lai and So [1]:

$$\frac{\partial}{\partial x_j}\left(\frac{\bar{\mu}}{Pr}\overline{u_i'\frac{\partial h'}{\partial x_j}}\right)+\frac{\partial}{\partial x_j}(\overline{h'\tau_{ij}'})$$

$$=\frac{\partial}{\partial x_j}\left(\frac{\bar{\mu}}{Pr}\frac{\partial \widetilde{u_i'h'}}{\partial x_j}\right)+\frac{\partial}{\partial x_j}\left(\bar{\mu}\frac{\partial \widetilde{u_i'h'}}{\partial x_j}\right). \quad (29)$$

Away from the wall the dissipation term is weak, a result which is also confirmed by the order of magnitude analysis of Mompean [2]. But, near the wall this term plays an important role in balancing the molecular diffusion term. It is modelled as follows:

$$\overline{\frac{\mu}{Pr}\frac{\partial u_i'}{\partial x_j}\frac{\partial h'}{\partial x_j}}+\overline{\tau_{ij}'\frac{\partial h'}{\partial x_j}}$$

$$=fw\bar{\rho}\left(\frac{1}{Pr}C_\mu\omega\widetilde{u_i'h'}+C_\mu\omega\widetilde{u_k'h'}n_kn_i\right). \quad (30)$$

The boundary conditions for the turbulent heat fluxes are now described.

4. BOUNDARY CONDITIONS

At the wall, the velocity fluctuations vanish so that we have the conditions:

$$\widetilde{u'h'}=0 \quad \widetilde{w'h'}=0 \quad (31)$$

At the outflow and the far-field border of the computational domain, Neumann conditions are used:

$$\frac{\partial \widetilde{u'h'}}{\partial x}=0 \quad \frac{\partial \widetilde{w'h'}}{\partial x}=0$$

$$\frac{\partial \widetilde{u'h'}}{\partial z}=0 \quad \frac{\partial \widetilde{w'h'}}{\partial z}=0 \quad (32)$$

The inflow border needs profiles of the mean primitive variables and the correlations. The boundary layer program (EDDYBL) of Wilcox [7] is used to compute most of the quantities. It does not, however, provide the turbulent heat fluxes. The simplest way to compute them at the inflow border is to use a gradient transport hypothesis of the form:

$$\bar{\rho}\widetilde{u'h'}=-\frac{\mu_t}{Pr\,t}\frac{\partial \tilde{h}}{\partial x}$$

$$\bar{\rho}\widetilde{w'h'}=-\frac{\mu_t}{Pr\,t}\frac{\partial \tilde{h}}{\partial z}. \quad (33)$$

This assumption can, however, cause problems, because the mean temperature gradient is almost zero in the mean flow direction. On the other hand, Lai and So's computations [1] predict heat fluxes in this direction, the magnitude of which is twice as large as that of the wall normal fluxes. The same trend is also found in boundary layer experiments of Fulachier [15]. In order to evaluate the influence of the boundary condition (33) on the longitudinal heat flux, a comparison is made between results based on (33) and those for which $\bar{\rho}\widetilde{u'h'}$ has been taken equal to $-2\bar{\rho}\widetilde{w'h'}$ at the inflow border.

5. NUMERICAL METHOD

The Favre-averaged Navier–Stokes equations for statistically two-dimensional flow and the transport equations for four Reynolds stress components, two turbulent heat fluxes and the ω-equation are solved with a finite volume method [16]. The convective fluxes in these equations are computed using an approximate one-dimensional Riemann solver. Van Albada type sensors serve to detect shock discontinuities. The diffusive terms are discretized by central differencing at each cell face. Source terms in the turbulence transport equations are calculated via central differences from the Riemann solution at the cell faces (Haidinger [4]). A first order implicit scheme is used for time-integration. Local time-stepping and weak coupling between the averaged Navier–Stokes and the turbulence transport equations help to save computer time and avoid stiffness problems [4, 5].

6. NUMERICAL RESULTS

The model is first applied to supersonic boundary layers along adiabatic walls at different Mach numbers (from 0.3 to 8). Then boundary layers on a cooled wall at a Mach number equal to 5 are considered. The ratio between the adiabatic temperature and the wall temperature varies from 0.3 to 1. Those test cases were proposed by Bradshaw *et al.* [17] in 1991 at the occasion of the project 'Collaborative testing of turbulence models'. Different groups of researchers have collaborated in this project and the goal was to evaluate different turbulence models by comparing the evolution of the skin friction as function of the Mach number in the first case and as function of the temperature ratio in the second case. Those test cases have been chosen in order to study and to compare the behaviour of the different parts of the new equations. Comparisons with results obtained with the Boussinesq hypothesis for the heat fluxes and with theoretical results are presented. Then, interactions of shocks with boundary layers are computed to test the modelled equations in more complex cases.

6.1. *Computation of boundary layers at different Mach numbers*

All the computations are made on meshes of 70×40 nodes in main and wall normal flow directions which were refined near the wall.

6.1.1. *Boundary layer at low Mach number.* A boundary layer at a subsonic Mach number is first computed. Since the transport equations for the turbulent heat fluxes have been modelled as for incom-

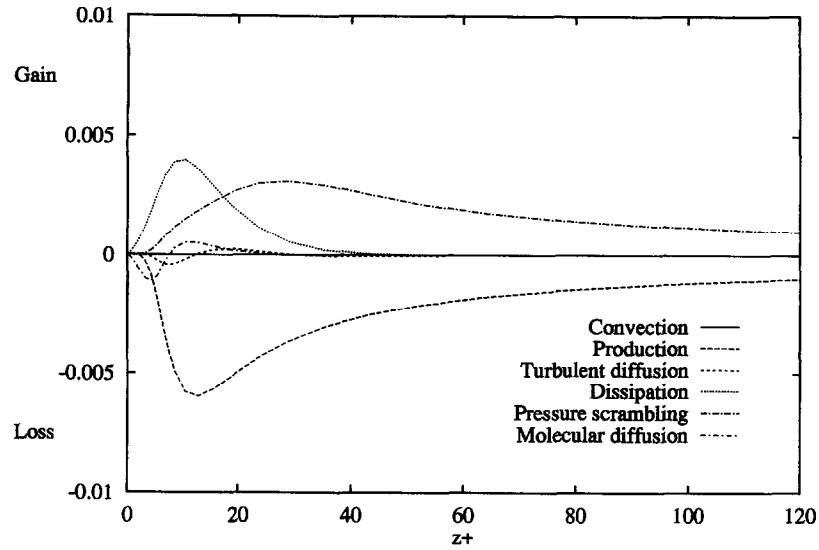

Fig. 1. Balance of streamwise turbulent heat flux in the wall layer of a $Ma = 0.3$ boundary layer (adiabatic wall).

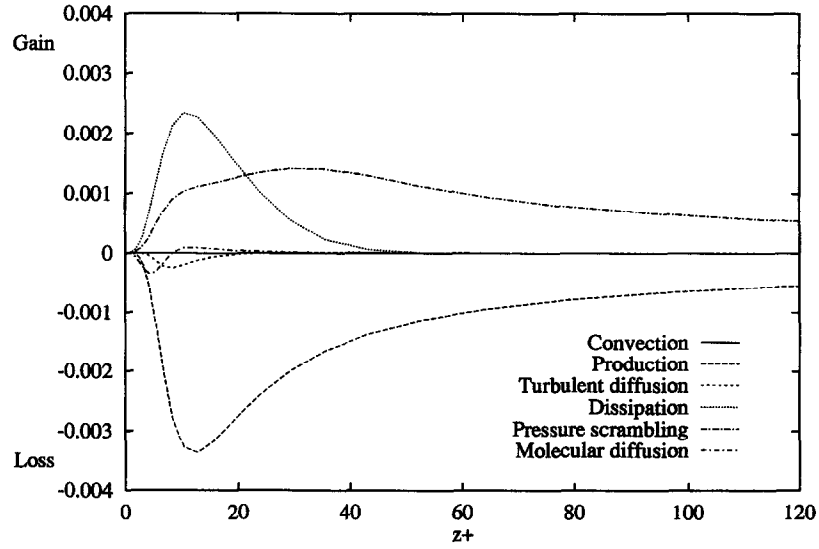

Fig. 2. Balance of wall-normal turbulent heat flux in the wall layer of a $Ma = 0.3$ boundary layer (adiabatic wall).

pressible flows, it is important to test the behaviour of the different terms in this test case first. As the numerical method is adapted to compressible flows, it is difficult to do a computation at a Mach number strictly equal to zero. A computation at a Mach number of 0.3 is thus performed.

The behaviour of the terms contributing to the balance of the turbulent heat fluxes $\widetilde{u''h''}$ and $\widetilde{w''h''}$ near the wall is presented in Figs. 1 and 2. For this first computation, the compressible terms 5 and 6 are not taken into account. The dissipation and the molecular diffusion play an important role near the wall and are very small away from the wall. The contribution of the turbulent diffusion is relatively weak and convection is insignificant. From z^+ greater than 40 onwards, equilibrium prevails between the production and pressure scrambling terms and the other terms are negligible. The profiles of the different terms are in good agreement with those of Lai and So [1] who have performed computations in the case of incompressible pipe flow.

To check if the models for the compressible terms make a contribution when the Mach number is weak, a computation with those terms is also performed. As

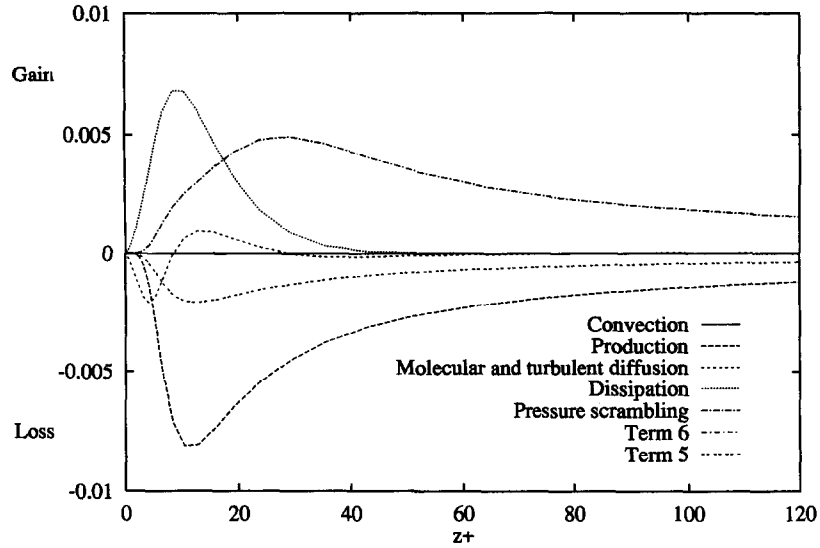

Fig. 3. Influence of terms 5 and 6, of equation (11), on the streamwise heat flux balance in the wall layer of a $Ma = 0.3$ boundary layer (adiabatic wall).

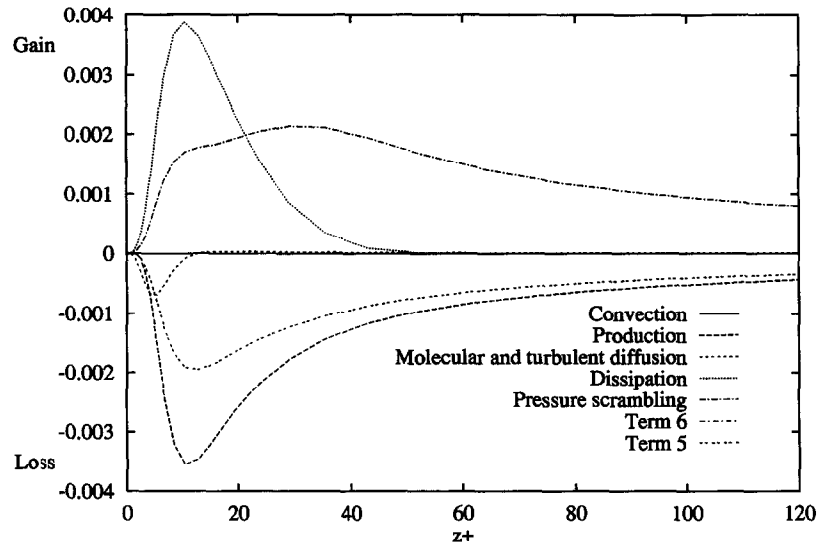

Fig. 4. Influence of terms 5 and 6, of equation (11), on the wall-normal heat flux balance in the wall layer of a $Ma = 0.3$ boundary layer (adiabatic wall).

one can see in Figs. 3 and 4, the term 5 contributes to equilibrium in a large part of the boundary layer, even at a weak Mach number. This modelisation is then dropped for the moment. The term 6 has practically no importance in the whole boundary layer.

6.1.2. *Boundary layer at Mach* 3. Different computations have then been performed, first to test the influence of the inlet boundary conditions for the heat fluxes and secondly to test the different options of the model. A Mach number of three has been chosen because it is of the order of magnitude of the Mach number of the boundary layer/shock wave interactions which are presented in the next section.

The inlet boundary conditions for equation (11) have first been computed with the gradient transport hypothesis, equation (33). However, for the $\widetilde{u'h'}$ correlation, this hypothesis is in contradiction with the computations. The computation predicts values of $\widetilde{u'h'}$ of the same order of magnitude as $\widetilde{w'h'}$ and the hypothesis of equation (33) predicts very low values because the temperature gradient in the longitudinal direction is weak. To test the influence of those boundary conditions on the results, two computations are performed. In the first case, hypothesis (33) is used to compute the inlet conditions and in the second case this condition is kept for $\widetilde{w'h'}$, but the condition $\widetilde{u'h'} = -\widetilde{w'h'}$ is imposed for $\widetilde{u'h'}$. The skin friction coeffic-

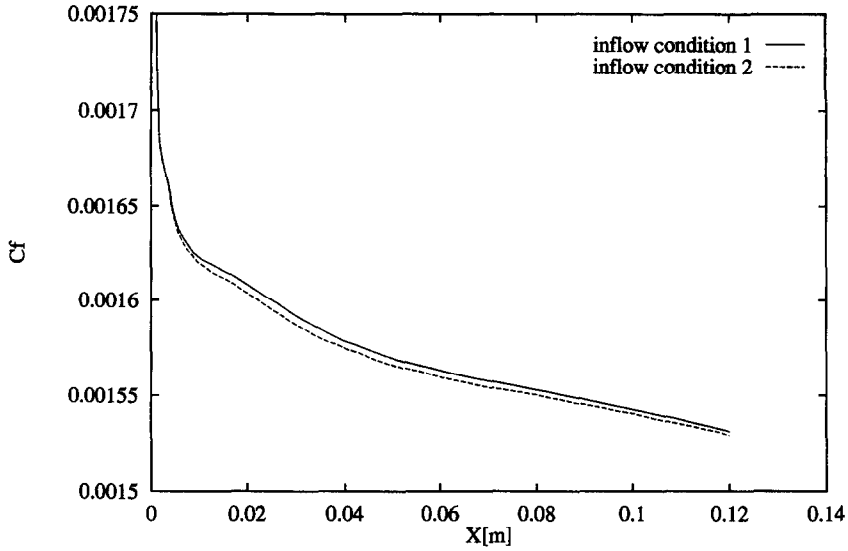

Fig. 5. Effect of inflow boundary conditions for the turbulent heat fluxes on the skin-friction development ($Ma = 3$ boundary layer, adiabatic wall).

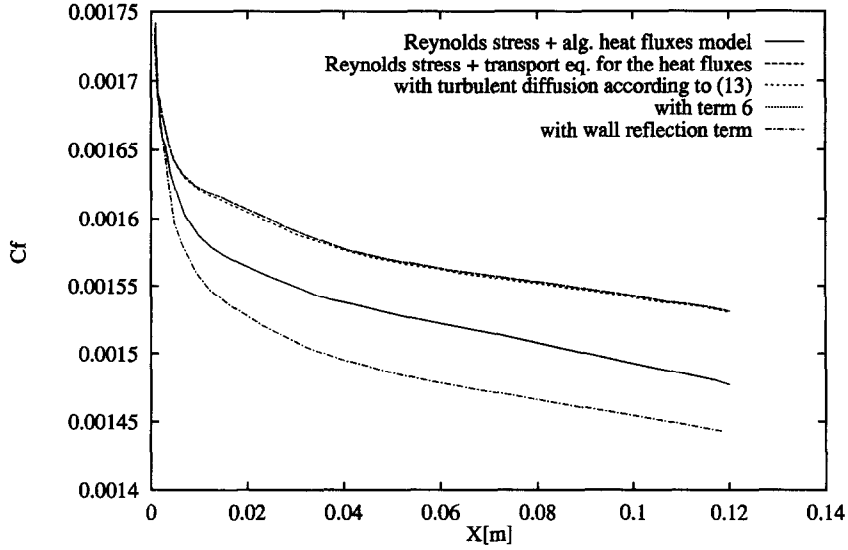

Fig. 6. Influence of different models in the computation of turbulent heat fluxes on the skin-friction development ($Ma = 3$ boundary layer, adiabatic wall).

ients predicted by the two cases are plotted in Fig. 5. We observe that the inlet condition has a very weak influence on the skin friction computation. In the future, the relation $\widetilde{u'h'} = -\widetilde{w'h'}$ is therefore retained at $x = 0$.

Then, the different options in the turbulent heat flux equations (turbulent diffusivity, compressibility term 6, wall reflection term) are tested and compared with the algebraic model in order to select the best one (Fig. 6). The formulation for the turbulent diffusion has a very small influence on the skin friction. The second formulation will be used in future, because it is more compatible with the one used in the Reynolds stress model. The compressibility term 6 also has a very weak influence. The wall reflection term, which is a part of the pressure-scrambling term, has a stronger effect and predicts a too weak skin friction: therefore it is not used in the future.

The balance of the heat flux transport near the wall is now presented in Figs. 7 and 8, in order to see the differences to the subsonic behaviour. We notice that the order of magnitude of the heat fluxes is greater than in the subsonic case because there is a temperature gradient near the wall which induces an increase in the production term. The gradient transport hypothesis predicts the same effect because its

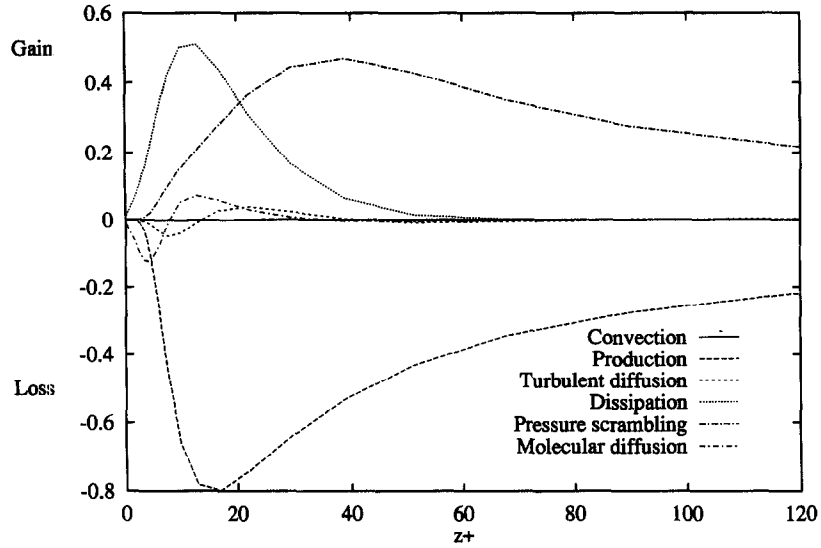

Fig. 7. Balance of the streamwise turbulent heat flux for a $Ma = 3$ boundary layer (adiabatic wall).

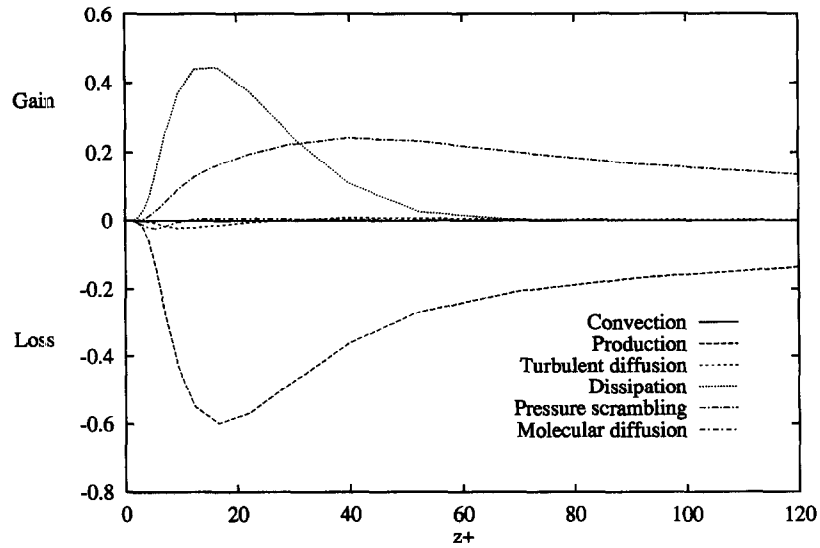

Fig. 8. Balance of the wall-normal turbulent heat flux for a $Ma = 3$ boundary layer (adiabatic wall).

correlations are proportional to the temperature gradient. If we compare the profiles of the different terms in the heat flux equations, we notice that the pressure scrambling term has a weaker effect near the wall than in the subsonic case. This term is proportional to the density which decreases near the wall in the case of a compressible flow.

In order to study the influence of the turbulent heat flux models (algebraic model, transport equations) on the mean field variables, the profiles of the different quantities (velocity, turbulent kinetic energy, turbulent heat fluxes etc.) are presented. All the profiles are plotted in the middle of the computational domain. The profiles of velocity and of kinetic energy (Figs. 9 and 10) are not modified much by the new model. The variations are more important for the temperature profile (Fig. 11). Finally, the turbulent heat fluxes computed from the transport equations are compared with the gradient transport hypothesis for $\widetilde{w'h'}$. Figure 12 contains profiles of $\widetilde{u'h'}$, $\widetilde{w'h'}$ normalized with the edge velocity and temperature. The level predicted by the algebraic model is higher than that predicted by the transport equations, at least of $\widetilde{w'h'}$. Experimental results to determine the reliability of these predictions are missing. Concerning $\widetilde{u'h'}$, the result for the algebraic model is not plotted because it is almost equal to zero. We also notice that the level

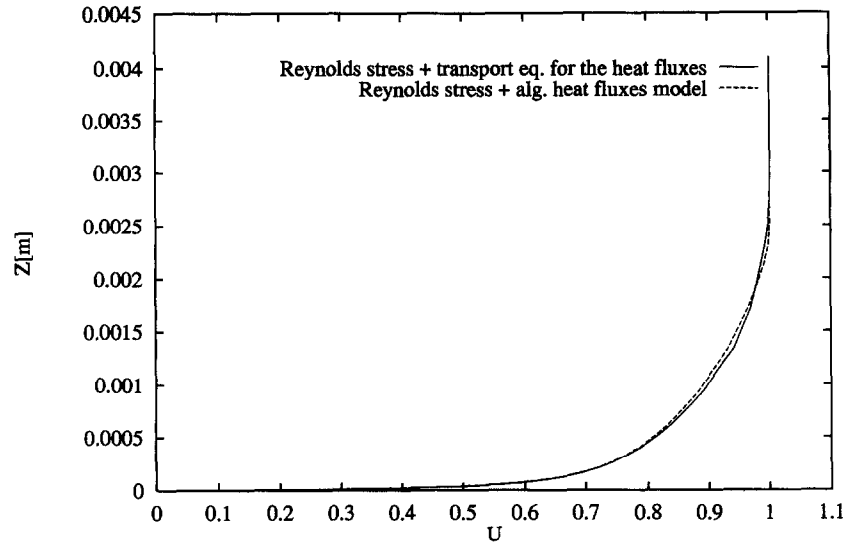

Fig. 9. Influence of heat flux models on mean longitudinal velocity ($Ma = 3$ boundary layer, adiabatic wall).

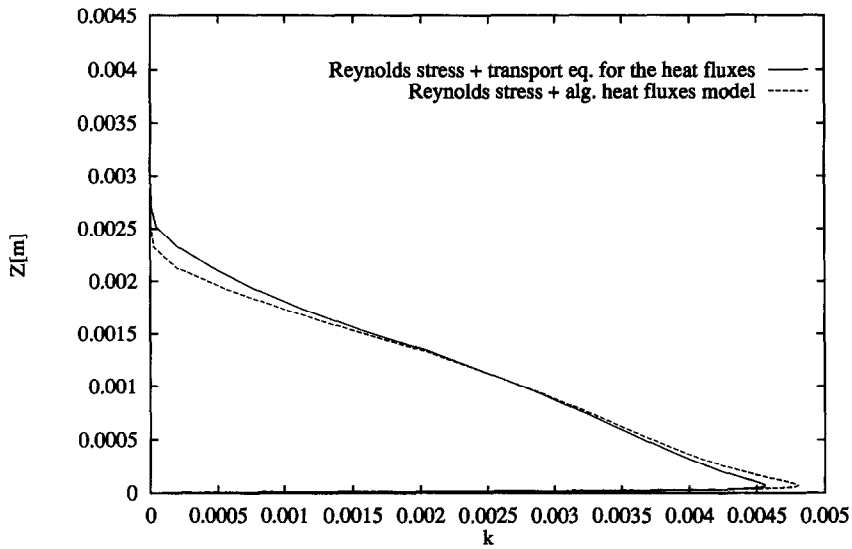

Fig. 10. Influence of heat flux models on turbulent kinetic energy ($Ma = 3$ boundary layer, adiabatic wall).

of $-\widetilde{u''h''}$ is higher than that of $\widetilde{w''h''}$, this is also true in the case of the incompressible pipe flow by Lai and So [1] and the boundary layer flow of Fulachier [15].

Figure 13 presents temperature profiles for two different positions ($R_\theta = 7040$ and $R_\theta = 9233$). We notice a temperature rise with the thickening of the boundary layer. It is most probably due to dissipation effects which heat the boundary layer and it explains why the turbulent heat fluxes are negative in the longitudinal direction. In the Reynolds stress model the production terms are only functions of the velocity gradients, but in the heat flux equations they are also functions of the temperature gradient. The temperature gradient has a behavior which differs from that of the velocity gradient. The velocity gradient has very high values near the wall and then decreases rapidly. On the contrary, the temperature gradient keeps values relatively high away from the wall. For low Reynolds number models, all the meshes are usually such that grid points are concentrated near the wall. When the temperature gradient has high values in the coarse grid region, oscillations in the profiles may appear. This means that relatively high resolution of the whole flow field is needed (especially also near the boundary layer edge) in order to avoid spacial oscillations in the temperature profile.

6.1.3. *Variation of skin friction with Mach number.* In order to study the dependency of the skin friction

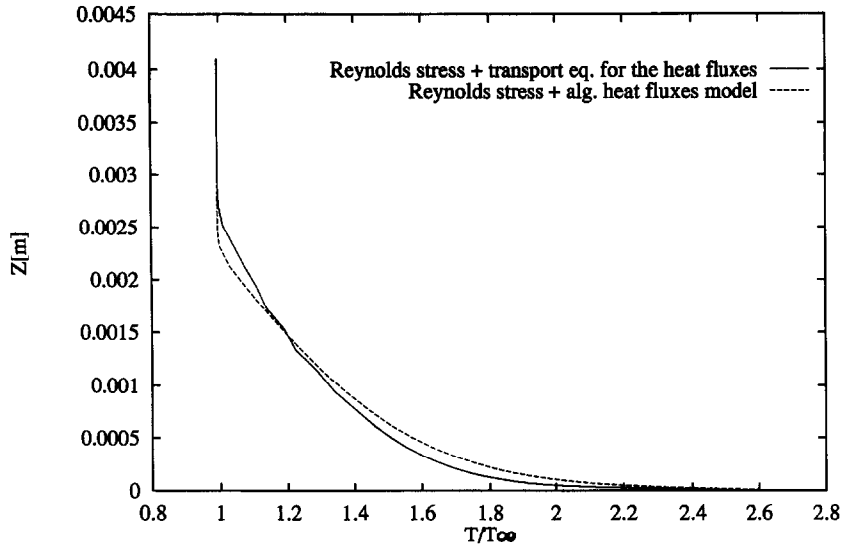

Fig. 11. Influence of heat flux models on mean temperature ($Ma = 3$ boundary layer, adiabatic wall).

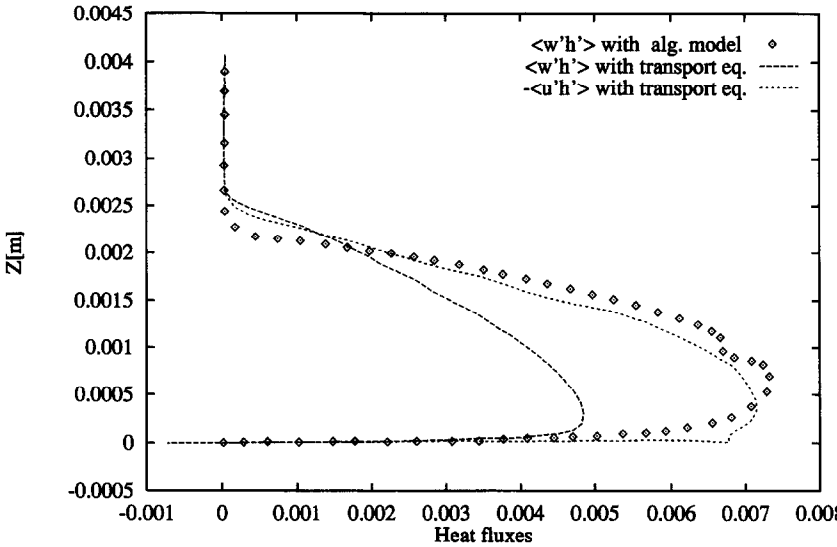

Fig. 12. Influence of heat flux models on turbulent heat flux profiles ($Ma = 3$ boundary layer, adiabatic wall).

coefficient on the Mach number, boundary layers with different Mach numbers (ranging from 1 to 8) are computed. The results are compared with the skin friction values obtained from the Van Driest correlation [18]. Studies have proved that this formula is in good agreement with experimental results in the case of compressible boundary layers [19]. The evolution of the skin friction coefficient with the Mach number is plotted in Fig. 14 for the two turbulence models and the Van Driest correlation. Table 1 contains the corresponding values of the skin friction. The results are close to Van Driest's values, except for Mach 8. At this Mach number, however, the limits of the efficiency of the solver are reached.

6.2. *Computation of boundary layers on a cooled wall*

Boundary layer computations for a cooled wall, at a Mach number of five are now presented. The ratio between the wall temperature imposed and the adiabatic temperature varies from 1.0 to 0.2.

The balance between the different terms in the turbulent heat flux equations is first presented in Figs. 15 and 16. Indeed, the cooling produces a sharp decrease in temperature near the wall and the temperature gradient changes its sign. This leads to a change of sign in the production and dissipation terms near the wall ($z^+ \approx 10$). As a further effect the maximum amplitudes of production, dissipation and pressure-scrambling terms are reduced compared to the adia-

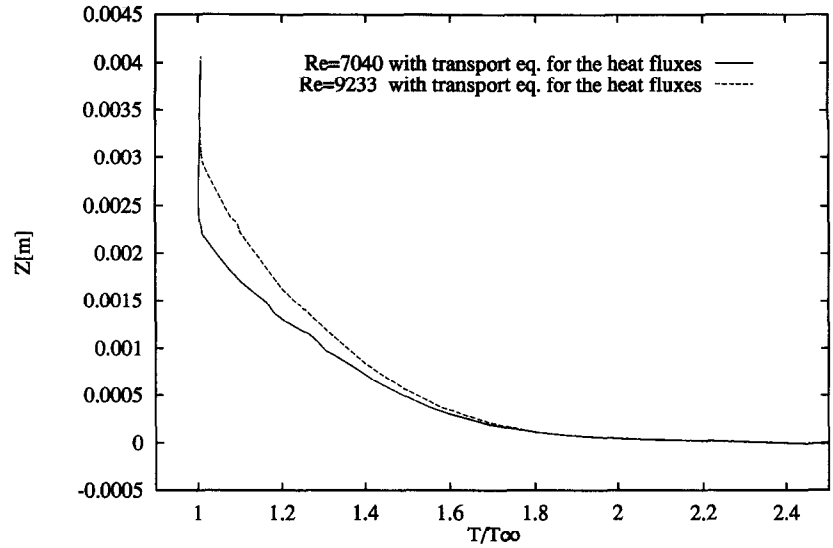

Fig. 13. Temperature profiles at different downstream positions ($Ma = 3$ boundary layer, adiabatic wall).

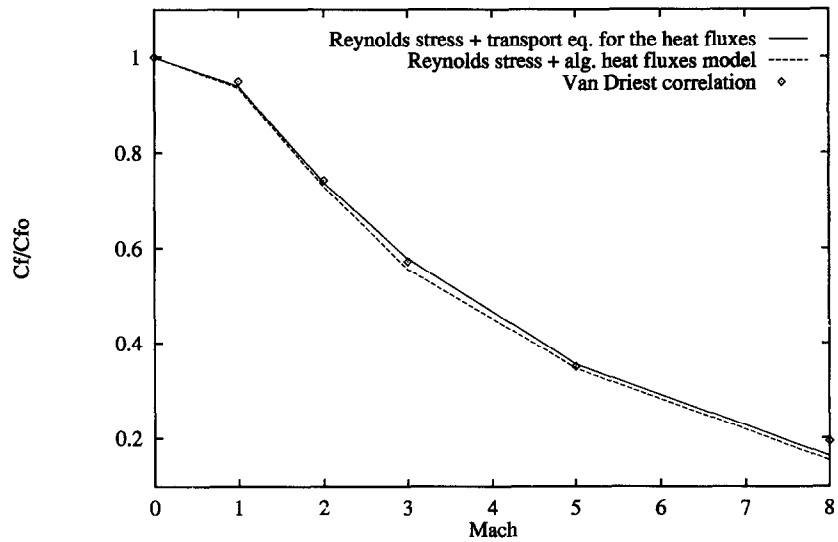

Fig. 14. Variation of skin friction coefficient with Mach number for the two turbulence models (boundary layer along adiabatic wall).

Table 1. Effect of turbulence model on skin friction for flat plate boundary layer along adiabatic wall

Skin friction (adiabatic wall)					
Mach number	0.3	2	3	5	8
Reynolds stress model & alg. model for heat fluxes	0.00268	0.00195	0.00149	0.000929	0.000418
Reynolds stress model & transport equation for heat fluxes	0.00277	0.00197	0.00155	0.000954	0.000436
Van Driest correlation	0.00267	0.00198	0.00153	0.000938	0.000518

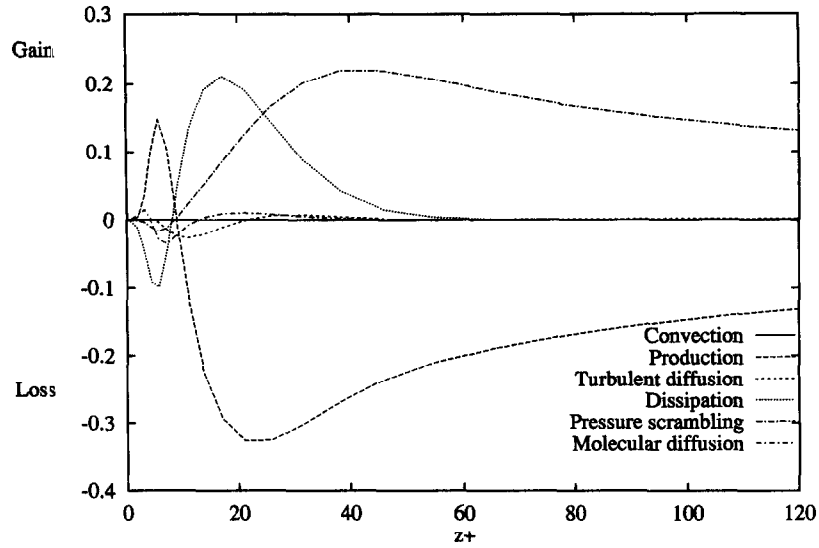

Fig. 15. Balance of streamwise turbulent heat flux for a $Ma = 5$ boundary layer along a cooled wall ($T_w/T_{ad} = 0.2$).

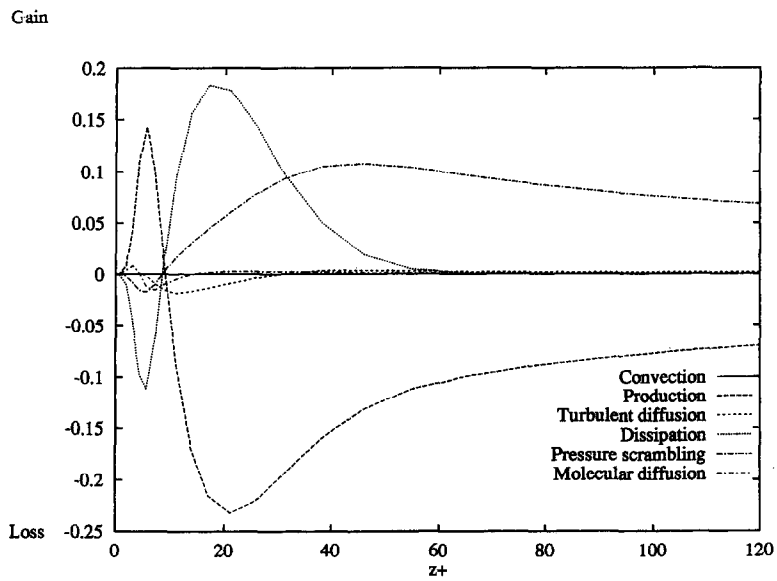

Fig. 16. Balance of wall-normal turbulent heat flux for a $Ma = 5$ boundary layer along a cooled wall ($T_w/T_{ad} = 0.2$).

batic wall case at $Ma = 3$. An explanation for all these effects must be searched for in the modified behaviour of the turbulent heat fluxes. The fact that these fluxes enter the models for the pressure-scrambling and dissipation terms underlines the importance of modeling in the near-wall region.

In order to compare the effects of wall cooling and thermal isolation on the turbulent heat fluxes at $Ma = 5$, Fig. 17 contains profiles of $\widetilde{u''h''}$ and $\widetilde{w''h''}$ for an adiabatic wall and for a ratio of $T_w/T_{ad} = 0.2$. The profiles show a reduction in the peak heat fluxes by factors of 2–3 in the case of wall cooling. Close to the wall the direction of both fluxes is reversed, which is a consequence of the change in the temperature gradient there, as to be seen in Fig. 18.

Comparisons are now made between the computed skin friction coefficients and the theoretical values of the Van Driest formula. The skin friction coefficient is non-dimensionalised by its incompressible value. The comparisons are presented in the Table 2 and in Fig. 19. The present computations are in good agreement with the Van Driest predictions.

6.3. *Computation of shock/boundary layer interactions*

To test the model in more complex cases, two interactions of boundary layers with shocks are computed.

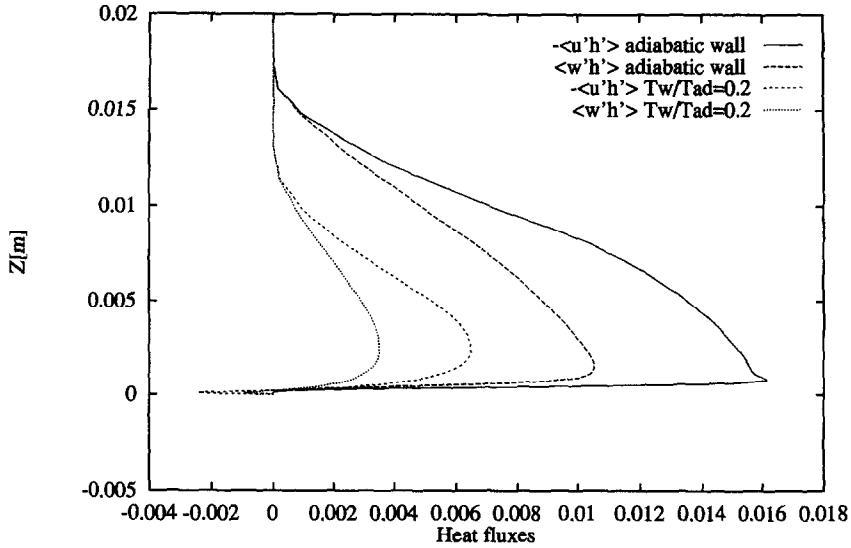

Fig. 17. Comparison between turbulent heat fluxes in a $Ma = 5$ boundary layer along an adiabatic wall and a cooled wall ($T_w/T_{ad} = 0.2$).

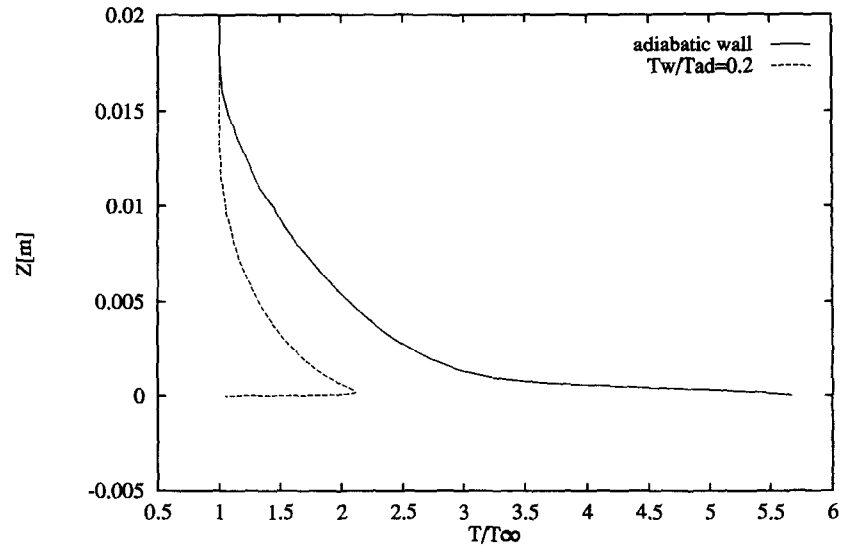

Fig. 18. Temperature profiles of $Ma = 5$ boundary layers along adiabatic respectively cooled walls ($T_w/T_{ad} = 0.2$).

Table 2. Effect of turbulence model on skin friction for flat plate boundary layer along cooled wall

	Skin friction (cooled wall)			
Temperature ratio T_w/T_{aw}	0.2	0.4	0.6	0.8
Reynolds stress model & alg. model for heat fluxes	0.001524	0.001297	0.001130	0.001030
Reynolds stress model & transport equation for heat fluxes	0.001507	0.001300	0.001154	0.001055
Van Driest correlation	0.001556	0.001321	0.001156	0.001038

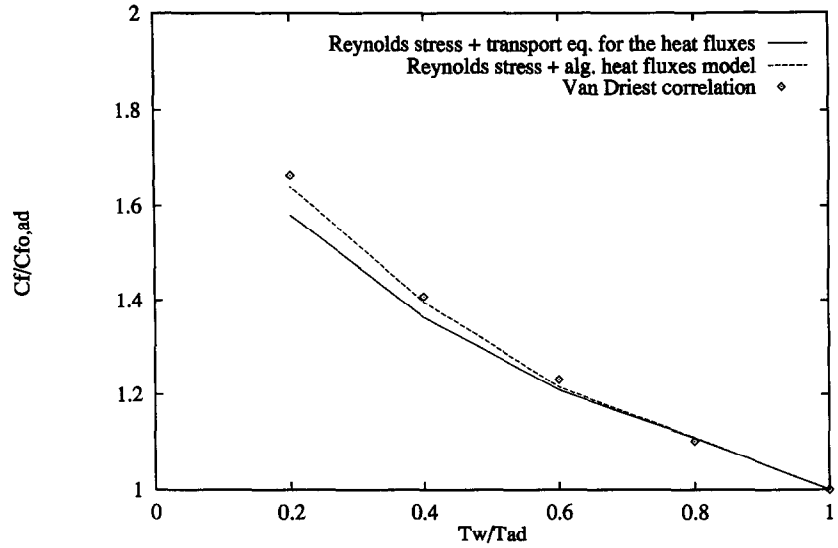

Fig. 19. Variation of skin friction coefficient with ratio of wall temperature to adiabatic wall temperature for a $Ma = 5$ boundary layer. Comparison of turbulence models with Van Driest correlation.

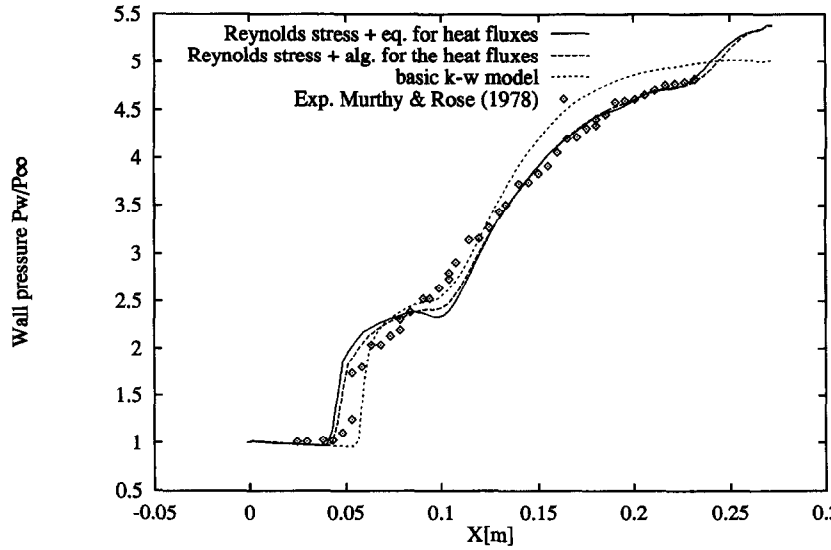

Fig. 20. Wall pressure distribution for oblique shock/boundary layer interaction. Comparison of three turbulence models ($Ma = 2.9$, $Re_\delta = 9.7 \times 10^5$, adiabatic wall).

The reflexion of an oblique shock on a boundary layer at $Ma = 2.9$ (the case of Reda and Murphy [20]) is first considered, then the interaction between a boundary layer and a shock caused by a 24° ramp at $Ma = 2.84$ (experiment of Settles *et al.* [21]). In the two cases, the strength of the shock is sufficient to produce a recirculation bubble. The computations are initialised with the results for the same flows obtained with the Reynolds stress model and the algebraic model for the heat fluxes. In the two cases, grids of 100×60 nodes refined near the wall are used. The profiles for wall pressure (Figs. 20 and 22) and skin friction (Figs. 21 and 23) are plotted. The results produced by the k–ω model, the Reynolds stress model with the algebraic heat fluxes and the Reynolds stress model with the transport equations for the heat fluxes are compared. The change from the k–ω model to the Reynolds stress model improves the results a lot in the case of the ramp flow (Figs. 22 and 23). However, the use of transport equations for the heat fluxes does not modify the results much compared to the algebraic model. We only notice a slight increase in the size of the recirculation bubble for the ramp flow. The reason is that the turbulent heat fluxes do not directly influence quantities like the wall pressure and the skin friction. A comparison of Stanton numbers would

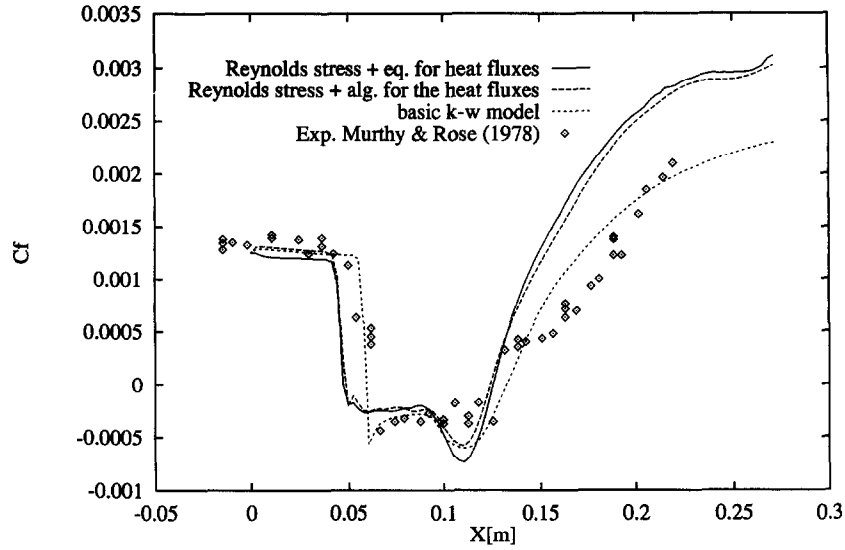

Fig. 21. Skin friction distribution for oblique shock/boundary layer interaction. Comparison of three turbulence models ($Ma = 2.9$, $Re_\delta = 9.7 \times 10^5$, adiabatic wall).

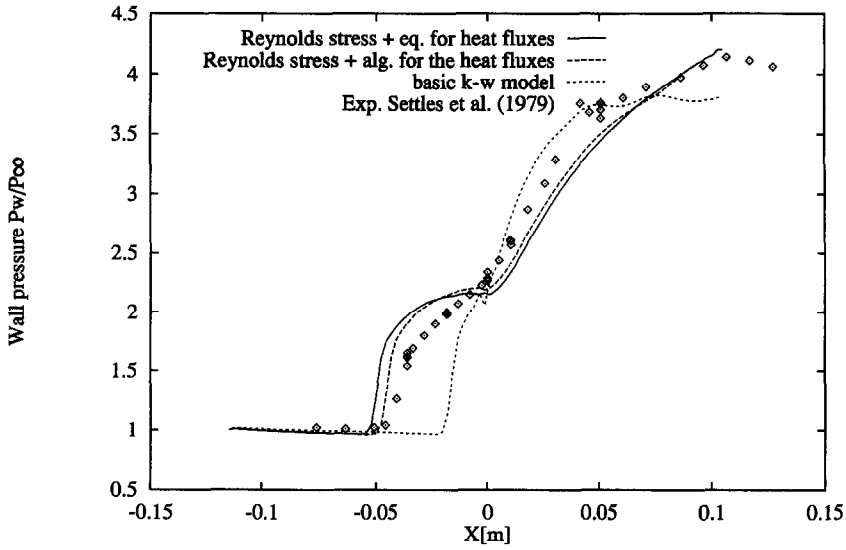

Fig. 22. Wall pressure distribution for 24° compression corner flow. Comparison of three turbulence models ($Ma = 2.84$, $Re_\delta = 1.69 \times 10^6$, adiabatic wall).

have been more interesting. Unfortunately experimental data were not reported by the authors [20, 21].

7. CONCLUSIONS

Modelled transport equations for the turbulent heat fluxes have been used to compute supersonic flows. The model assumptions are very close to those of Lai and So [1] developed for incompressible flows. They should lead to reliable results as long as intrinsic effects of compressibility do not appear, i.e. for wall boundary layers up to $Ma = 5$ where compressibility effects can be interpreted in terms of mean density variations. The model must fail when remarkable density fluctuations appear in the flow as a consequence of high levels of the turbulent Mach number or more precisely of the gradient Mach number (see Sarkar [22]).

Several computations of simple boundary layers along isothermal and cooled walls at different Mach numbers have been performed. Such flow cases have also been used to test different inflow boundary conditions and model assumptions. It turns out that the use of heat flux equations does not modify much the aerodynamic field data as compared to algebraic heat flux models. The profiles of the turbulent heat fluxes, however, clearly differ from algebraic predictions. In

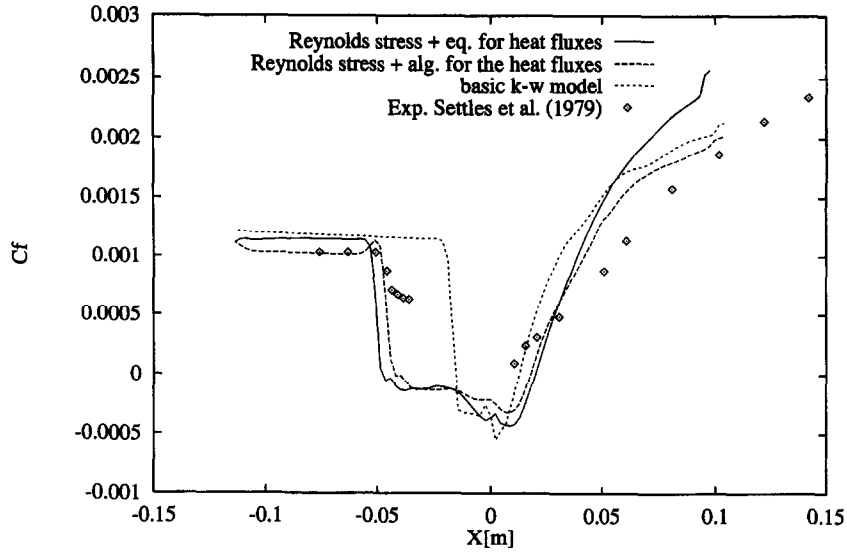

Fig. 23. Skin friction distribution of 24° compression corner flow. Comparison of three turbulence models ($Ma = 2.84$, $Re_\delta = 1.69 \times 10^6$, adiabatic wall).

particular, the longitudinal heat flux is wrongly predicted by the gradient transport hypothesis. Further evidence of the advantage of transport equations over algebraic models might be gained by comparing Stanton numbers. Unfortunately, they were not reported in the experiments used for reference. The skin friction and wall pressure distributions of shock turbulence interactions again do not show dramatic modifications due to the use of heat flux equations. This shows that new and careful experiments have to be carried out, in which, besides complete data of the turbulent momentum transport, detailed heat flux data are obtained. Only then, a conclusive evaluation of the present turbulence model is possible.

Acknowledgements—The authors are grateful to the German Research Association (DFG) for financially supporting this work within the collaborative Research Center SFB 255.

REFERENCES

1. Lai, Y. G. and So, R. M. C., Near-wall modeling of turbulent heat fluxes. *International Journal of Heat Mass Transfer*, 1990, **33**, 1429–1440.
2. Mompean Munhoz Da Cruz, G., Modélisation des écoulements turbulents avec transferts thermiques en convection mixte. Ph.D. thesis, Ecole Centrale de Lyon, France, 1989.
3. Sommer, T. P., So, R. M. C. and Lai, Y. G., A near-wall two-equation model for turbulent heat fluxes. *International Journal of Heat Mass Transfer*, 1992, **35**, 3375–3387.
4. Haidinger, F. A., Numerische Untersuchung turbulenter Stoss-/Grenzschicht-Wechselwirkungen. Ph.D. thesis, Technische Universität München, Germany, 1993.
5. Haidinger, F. A. and Friedrich, R., Computation of shock wave/turbulent boundary layer interactions using a Reynolds stress model. *Ninth Symposium on Turbulent Shear Flows*, Kyoto, Japan, 1993, pp. 4-3-1–6.
6. Haidinger, F. A. and Friedrich, R., Numerical simulation of strong shock/turbulent boundary layer interactions using a Reynolds stress model. *Zeitschrift für Fluwissenschaften und Weltraumforschung*, 1995, **19**, 10–18.
7. Wilcox, D. C., *Turbulence Modeling for CFD*. Griffin Printing, Glendale, CA 1993.
8. Zeman, O., Dilatational dissipation: the concept and application in modeling compressible mixing layers. *Physics of Fluids A*, 1990, **2**, 178–188.
9. Zeman, O. and Coleman, G. N., Compressible turbulence subjected to shear and rapid compression. *Turbulent Shear Flows* 8. Springer, Berlin, 1993, pp. 281–296.
10. Speziale, C. G., Sarkar, S. and Gatski, T. B., Modeling the pressure-strain correlation of turbulence: an invariant systems approach. *Journal of Fluid Mechanics*, 1991, **227**, 245–272.
11. Hanjalic, K. and Launder, B. E. A Reynolds stress model of turbulence and its application to thin shear flows. *Journal of Fluid Mechanics*, 1972, **52**, 609–638.
12. Sarkar, S., Erlebacher, G. and Hussaini, M. Y., Compressible homogeneous shear: simulation and modeling. *Eighth Symposium on Turbulent Shear Flows*, Munich, Germany, 1991.
13. Launder, B. E., Scalar property transport by turbulence. Report no. HTS/73/26, Department of Mechanical Engineering, Imperial College, London, 1973.
14. Speziale, C. G. and Sarkar, S., Second-order closure models for supersonic turbulent flows. AIAA Paper 91-0217, 1991.
15. Fulachier, L., Contribution à l'étude des analogies des champs dynamiques et thermique dans une couche limite turbulente. Effet de l'aspiration. Ph.D. thesis, Université de Provence, Marseille, France, 1972.
16. Schmatz, M. A., NSFLEX—An implicit relaxation method for the Navier–Stokes equations for a wide range of Mach numbers. MBB-report MBB-FE122-S-PUB-366, Messerschmitt–Bölkow–Blohm, Ottobrunn, Germany.
17. Bradshaw, P., Launder, B. E. and Lumley, J. P., Collaborative testing of turbulence models. AIAA-Paper 91 0215, 1991.
18. Van Driest, E. R., Problem of aerodynamic heating. *Aeronautical Engineering Review*, 1956, **15**, 26–41.
19. Hopkins, E. J. and Inouye, M., An evaluation of theories for predicting turbulent skin friction on flat plates at supersonic and hypersonic Mach numbers. *AIAA Journal*, 1971, **9**, 993–1003.

20. Reda, D. C. and Murphy, J. D., Shock wave-turbulent boundary layer interaction in rectangular channels. *AIAA Journal*, 1973, **11**, 139–140.
21. Settles, G. S., Fitzpatrick, T. J. and Bogdonoff, S. M., Detailed study of attached and separated compression corner flowfields in high Reynolds number supersonic flow. *AIAA Journal*, 1979, **17**, 579–585.
22. Sarkar, S., The stabilizing effect of compressibility in turbulent shear flow. *Journal of Fluid Mechanics*, 1995, **282**, 163–186.